



Nano-size defects in arsenic-implanted HgCdTe films: a HRTEM study

O. Yu. Bonchuk¹ · H. V. Savytskyy¹ · Z. Swiatek² · Y. Morgiel² · I. I. Izhnin^{3,4} · A. V. Voitsekhovskii⁴ · A. G. Korotaev⁴ · K. D. Mynbaev^{5,6} · O. I. Fitsych⁷ · V. S. Varavin⁸ · S. A. Dvoretzky^{4,8} · D. V. Marin⁸ · M. V. Yakushev⁸

Received: 27 December 2017 / Accepted: 8 February 2018 / Published online: 26 February 2018
© Springer-Verlag GmbH Germany, part of Springer Nature 2018

Abstract

Radiation damage and its transformation under annealing were studied with bright-field and high-resolution transmission electron microscopy for arsenic-implanted HgCdTe films with graded-gap surface layers. In addition to typical highly defective layers in as-implanted material, a 50 nm-thick sub-surface layer with very low defect density was observed. The main defects in other layers after implantation were dislocation loops, yet after arsenic activation annealing, the dominating defects were single dislocations. Transport (from depth to surface), transformation and annihilation of radiation-induced defects were observed as a result of annealing, with the depth with the maximum defect density decreasing from 110 to 40 nm.

Keywords HgCdTe · Arsenic implantation · Transmission electron microscopy · Nano-size defect

Background

Ion implantation is very widely used method for ex situ fabrication of p - n junctions for photodiodes based on $\text{Hg}_{1-x}\text{Cd}_x\text{Te}$ (MCT), an important material used for infrared photoelectronics. Currently, there is much interest in photodiode technology that is based on implantation of arsenic with fabrication of p^+ -type implanted region in n -type base

(Bommena et al. 2015; Gravrand et al. 2013; Izhnin et al. 2017a, b; Kerlain et al. 2016; Mollard et al. 2009, 2011). As dark currents in p - n junctions of the ' p^+ - n '-type are lower than those in ' n^+ - p '-type junctions, a higher working temperature or longer wavelength cut-off sensitivity threshold of photodiodes can be achieved with this architecture.

It is known that electrical properties of MCT straight after ion implantation are controlled by radiation defects rather than by the implanted species. Strong n -type doping is always registered in implanted MCT irrespective of the nature of implanted ions. This doping is caused by radiation defects, and to achieve p -type conductivity, the number of the defects should be reduced and implanted ions must be activated electrically. For this purpose, activation annealings are performed. The effect of such annealing has been studied mostly using electrical measurements and optical methods, while the data on the microstructure of the radiation-damaged area and its behavior under annealing are very limited (Lobre et al. 2013, 2014; Mollard et al. 2009, 2011). The knowledge of the nature of defects in the implanted region and of their evolution under annealing is, however, of much importance, as these defects can greatly affect the performance of p - n junctions and the lifespan of a photoelectronic device. The task of this work was to study the microstructure of MCT implanted with arsenic before and after activation annealing with high resolution, so nano-size defects could be observed and identified.

✉ O. Yu. Bonchuk
bonchuk@ukr.net

¹ Ya. S. Pidstryhach Institute for Applied Problems of Mechanics and Mathematics NASU, Naukova 3b, 79060 L'viv, Ukraine

² Institute of Metallurgy and Material Science PAN, Reymonta. 25, 30-059 Kraków, Poland

³ Scientific Research Company "Carat", Stryjska 202, 79031 L'viv, Ukraine

⁴ National Research Tomsk State University, Lenina 36, 634050 Tomsk, Russia

⁵ Ioffe Institute, Polytechnicheskaya 26, 194021 Saint Petersburg, Russia

⁶ ITMO University, Kronverkskiy 49, 197101 Saint Petersburg, Russia

⁷ Hetman Petro Sahaidachny National Army Academy, Gvardijska 32, 79012 L'viv, Ukraine

⁸ A.V. Rzhanov Institute of Semiconductor Physics, SB RAS, ac. Lavrentieva 13, 630090 Novosibirsk, Russia

Methods

We have studied HgCdTe epitaxial film grown with molecular-beam epitaxy (MBE) at A.V. Rzhanov Institute of Semiconductor Physics (Novosibirsk, Russia) on (013) CdTe/ZnTe/Si substrates with the growth cycle controlled in situ by means of an ellipsometer (Yakushev et al. 2011). The ‘absorber’ layer of the film had constant composition (CdTe molar fraction) $x = 0.221 \pm 0.002$; also, the film had graded-gap protective surface layer with composition at the surface approaching $x = 0.46$. The thickness of the graded-gap layer was ~ 400 nm. MCT was doped during the growth with In with concentration $\sim 5 \times 10^{15} \text{ cm}^{-3}$, so as-grown film had n -type conductivity with electron concentration and mobility as measured at 77 K $3.9 \times 10^{14} \text{ cm}^{-3}$ and $\mu_n = 87,500 \text{ cm}^2/(\text{V s})$, respectively.

Two similar samples cut from the same wafer were implanted with As^+ ions with energy 190 keV and ion fluence 10^{14} cm^{-2} . The implantation was performed using IMC200 (Ion Beam Services, France) system. After the implantation, one of the samples was subjected to two-stage thermal activation annealing in saturated mercury vapors (360 °C, 2 h and 220 °C, 24 h). The first high-temperature stage was performed to reduce the radiation damage and to activate implanted arsenic, while the second, low-temperature stage was used to annihilate mercury vacancies generated during the growth, ion implantation, and the first annealing stage. Thus, after the annealing, the extrinsic n -type due to indium doping was restored. Arsenic secondary-ion mass-spectroscopy (SIMS) profiles were recorded using Cameca IMS-6F (France) machine with As detection limit $\sim 1 \times 10^{16} \text{ cm}^{-3}$.

The microstructure observations were performed in bright-field transmission electron microscopy (BF TEM) and high-resolution transmission electron microscopy (HRTEM) modes using Tecnai G2 F20, FEI Company microscope. Thin foils for TEM and HRTEM observations were cut out using FEI Quanta 200 dual beam focused ion beam (FIB) machine. The analysis of the HRTEM images was carried out using direct and reverse fast Fourier transforms (FFT, IFFT).

Results and discussion

Defect structure of the film after ion implantation

Ion implantation of rather heavy arsenic ions leads to strong radiation damage in sub-surface layer of MCT and extended structural defects of various sizes are formed. In the studied film, BF TEM studies revealed

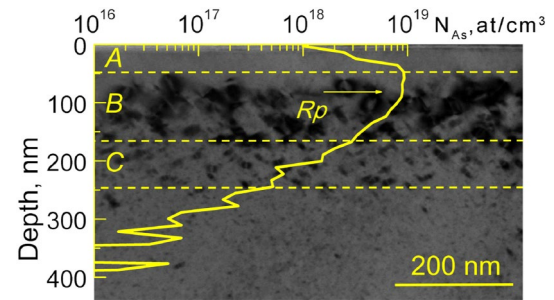


Fig. 1 Cross-sectional BF TEM image of radiation-damaged area in arsenic-implanted MCT film before annealing. Letters designate specific layers discussed in the text. Solid curve shows arsenic profile acquired with SIMS, R_p is projected ion range

radiation-damaged area with the total depth achieving ~ 250 nm. Figure 1 shows BF TEM image of a cleft edge of the radiation-damaged area after ion implantation. It is known that TEM is able to image extended defects but is not sensitive to point lattice deformations (Umeda et al. 2004). The defect pattern observed in Fig. 1 is typical of this type of experiment (see, e.g., Lobre et al. 2013, 2014; Mollard et al. 2009, 2011). Also, it appeared that according to SIMS data, the profile of the implanted ions extended to the depth ~ 350 nm (with projected range $R_p \sim 93$ nm), and thus, was completely located within the graded-gap protective surface layer. The arsenic profile is also shown in Fig. 1.

According to BF TEM data, the defect area in Fig. 1 contains three types of layers, which differ in the character and concentration of defects:

1. Layer **A** with thickness 50 nm; arsenic ions seem to penetrate this layer without bringing substantial damage to the material;
2. Layer **B** with thickness 120 nm, which contains large extended defects;
3. Layer **C** with thickness 80 nm; this is a transition layer bordering with the layer containing quasi-point radiation defects, which cannot be revealed in BF TEM mode.

Layer **A** contains much less defects than layers **B** and **C** do. TEM image of layer **A** shows only small clusters of defects, which are probably formed by vacancies and implanted ions. Layer **A** also contains stacking faults and nano-twins. They are shown in Fig. 2, which represents a HRTEM image of a certain region in this layer. Yellow dotted line highlights the defect structure that is typical of this layer, and inset in Fig. 2 shows FFT pattern of the highlighted area. Blurriness and repetition of diffraction spots (shown with circles) clearly indicate the presence of stacking faults and nano-twins. Thus, layer **A** with the minimum concentration of defects contains dislocations, small

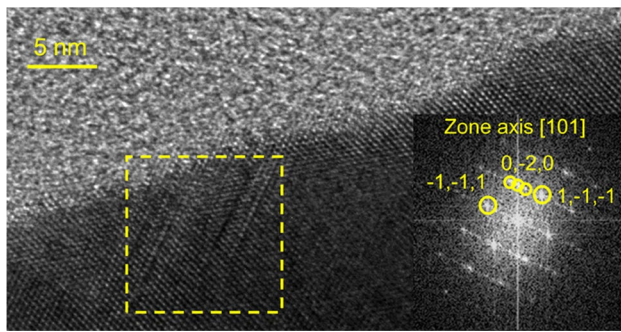


Fig. 2 HRTEM image of a small region in layer A. Inset shows FFT pattern of the part of the image highlighted with yellow dotted line

defect clusters (formed by vacancies, host atoms and dopant atoms), stacking faults and nano-twins. Generally speaking, the appearance of this clearly defined layer with low density of structural defects is not common. Indeed, such layer was not observed in similar MBE-grown MCT structures with removed graded-gap surface layer implanted with arsenic with 10^{15} cm^{-2} fluence and 190 keV energy (Izhnin et al. 2017b). However, Lobre et al. (2013) for liquid-phase epitaxy-grown homogeneous MCT film implanted with arsenic with 360 keV energy and low fluence ($5 \times 10^{13} \text{ cm}^{-2}$) observed a shallow zone with few defects with the depth of about 40 nm under the surface, while for $2 \times 10^{14} \text{ cm}^{-2}$ fluence such zone was not detected.

Layer B has the highest concentration of extended defects, and these defects have largest sizes. This layer extends from the depth of 50 down to 170 nm (Fig. 1). In addition to many small defect clusters, this layer contains dislocation loops with various sizes; in fact, these loops are the dominating defects in this layer. For example, Fig. 3 shows dislocation

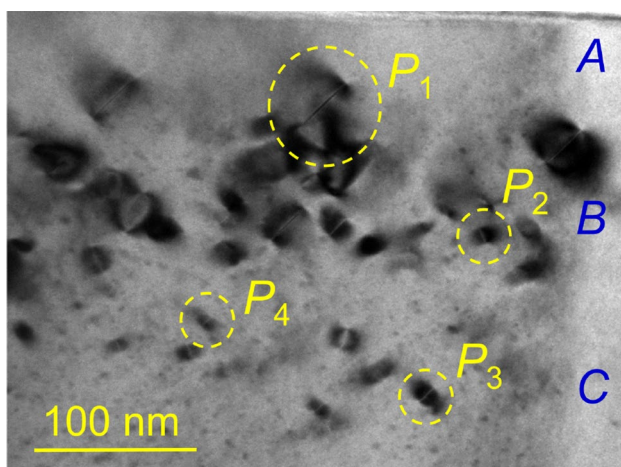


Fig. 3 Cross-sectional BF TEM image of structural defects at the interface of defect layers B and C. P1...P4 are specific regions exemplifying defect structure of these layers as discussed in the text

loops P1 and P2 with sizes 40 and 9 nm, respectively (compare to smaller loops P3 and P4 located in layer C). Figure 4 shows a HRTEM image of a vacancy-type dislocation loop with size 28 nm. During the implantation, smaller loops merge with formation of larger extended defects. The point with maximum concentration of the loops is located at the depth ~ 110 nm and is deeper than R_p . Such effect was also observed for the peak of the Rutherford backscattering (RBS) damage profiles obtained by Lobre et al. (2013): most arsenic ions were found around 150 nm under the layer surface, yet the depth of defect maxima was shifted deeper. According to Lobre et al. (2013), this confirms the ballistic effect of the implantation process. The shift was attributed to the weak ionic bonds of MCT, which allowed defects to propagate beyond the depth at which ions were stopped.

Transition layer C has lower, as compared to layer B, concentration of dislocation loops, and these loops are smaller in size (see, e.g., areas P3 and P4 in Fig. 3, where the loops have sizes of 7 and 12 nm, respectively). At the same time, concentration of defect clusters in this layer increases as compared to that in layer B (dark spots in Fig. 3).

Below the transition layer (see Fig. 1), there is a layer that does not contain extended radiation defects. This layer contains donor-like quasi-point radiation defects that are formed by interstitial mercury atoms, which are generated in the process of implantation and diffuse into the film. These defects cannot be resolved in BF TEM images, but appear as a uniform diffused background. As was shown by Izhnin et al. (2017a), the thickness of this layer depends on ion fluence. This layer also contains defect clusters (vacancy clusters and/or clusters containing gallium atoms used in FIB cutting).

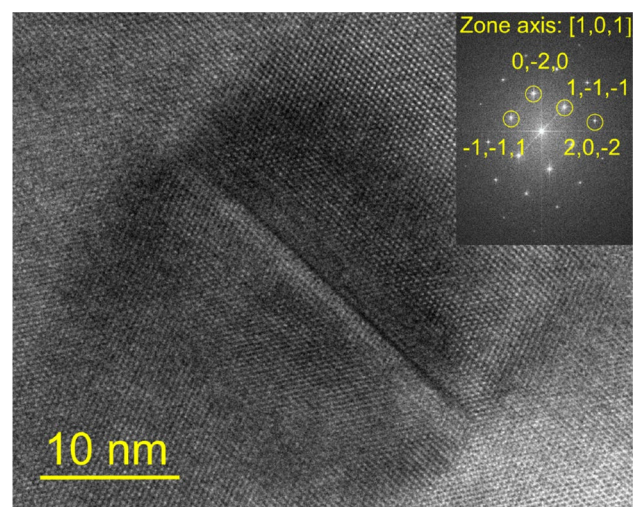


Fig. 4 HRTEM image of a separate dislocation loop in defect layer B. Inset shows FFT pattern of the image

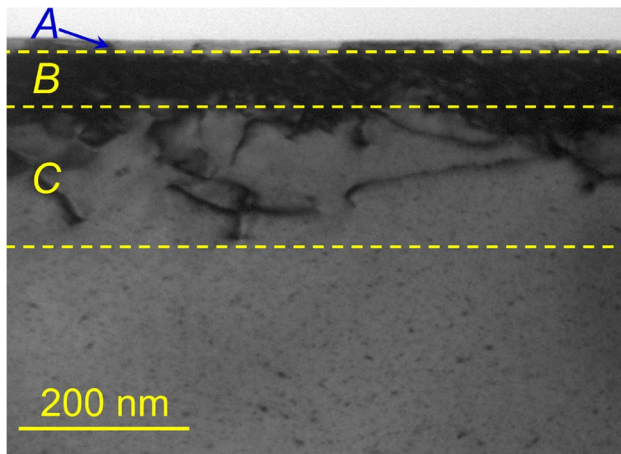


Fig. 5 Cross-sectional BF TEM image of radiation-damaged area in arsenic-implanted MCT film after activation annealing

Defect structure of the film after activation annealing

The effect of the annealing on the defect structure of radiation-damaged area is shown in Fig. 5, which presents a BF TEM image of a cleft edge of the film after ion implantation and activation annealing. Here one can distinguish three layers with various types of defects and their densities:

1. Layer **A** with thickness 10 nm, which contains dislocations with low density;
2. Layer **B** with thickness 60 nm, which contains dislocations with high density;
3. Layer **C** with thickness 170 nm; this is a transition layer bordering with the layer containing quasi-point radiation defects.

A distinctive feature of layer **A** in this case is the absence of visible dislocation loops. Figure 6 shows HRTEM image of layer **A**. In this layer, one can observe both areas containing dislocations and stacking faults (marked with arrows in Fig. 7a) and areas with almost ideal crystalline structure (Fig. 7b).

Figure 8a shows a HRTEM image of a small region in layer **B**. This region contains many dislocations and stacking faults. Dislocation density in this layer is $7.7 \times 10^9 \text{ cm}^{-2}$. Figure 8b shows inverse FFT image of the area designated in Fig. 8a with symbol I. One can see there an interstitial-type dislocation loop with 5 nm size (marked as P5), dislocations marked with arrows, and stacking faults between the dislocations (area marked as P6). Similar defects were observed for an area designated in Fig. 8a with symbol II.

Layer **B** is followed by layer **C** where both the density and the size of dislocation loops decrease. Similar to the non-annealed sample, layer **C** contains quasi-point defects: Fig. 5

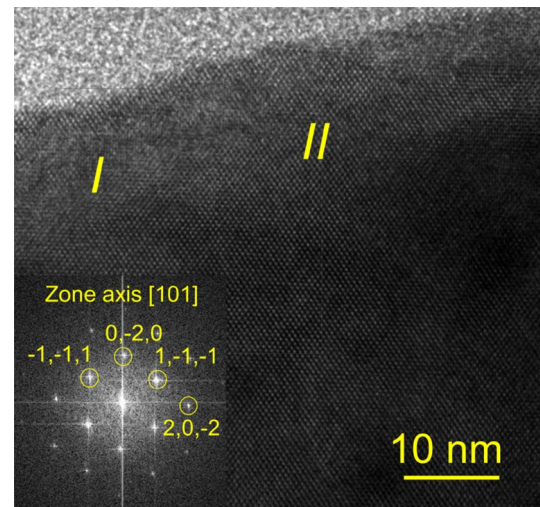


Fig. 6 HRTEM image of a small region in layer **A** after activation annealing. I and II indicate the areas under analysis (see text). Inset shows FFT pattern of the image

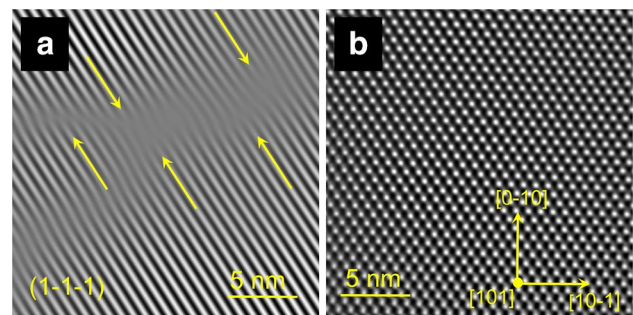


Fig. 7 Inverse FFT images of HRTEM image (Fig. 6) for areas I (a) and II (b)

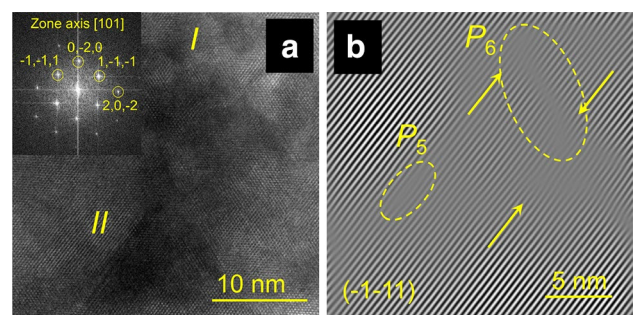


Fig. 8 HRTEM image of a small region in layer **B** after activation annealing (a). I and II indicate the areas of analysis. Inset shows FFT pattern of image (a). Related inverse FFT images for area II (b)

shows in this layer numerous clusters of defects, which are formed by vacancies, impurities, and/or gallium atoms, which penetrated into material during FIB cutting. As was

shown by Izhnin et al. (2017a), activation annealing resulted in complete annihilation of donor-like radiation defects.

Thus, after activation annealing, the defect structure of radiation-damaged area changes. Now, it mostly consists of a 60 nm-thick layer with dislocations (Fig. 5, layer B), whose maximum concentration is observed at the depth of 40 nm. In addition to dislocations, this layer also contains stacking faults and small dislocation loops. The layer with low density of dislocations (Fig. 5, layer A) has thickness of only 10 nm. The total thickness of all the defect layers after annealing is about 240 nm.

Comparing the defect structure of MCT films subjected to ion implantation only and to implantation and activation annealing, we can conclude the following. Despite the fact that the total thicknesses of defect layers in these two samples are similar (250 and 240 nm, respectively), the thicknesses and the depths of two major defect layers differ. After annealing, the thickness of the sub-surface layer with low concentration of extended defects (layer A) decreases from ~ 50 nm down to ~ 10 nm. The depth of the maximum concentration of defects in layer B moves towards the surface of the film (from ~ 110 nm up to ~ 40 nm), while its thickness reduces two-fold (from 120 nm down to 60 nm). At the same time, the thickness of transition layer C after annealing shows two-fold increase, from 80 nm up to 170 nm. These changes in defect structure after annealing result from a complicated process of reconstruction of the crystalline structure of the material, which proceeds from the depth of the defect region towards the surface of the film via transport, transformation and/or annihilation of radiation defects. This process is accompanied by dissociation of extended structural defects and by formation of dislocations. The reason for this is possibly generation, in the course of the annealing, of mercury interstitials. They diffuse into the crystal and interact with dislocation loops, which are mostly of vacancy-type, producing single dislocations. As a result, the whole defect region appears to be ‘moved’ towards the surface.

Conclusion

Bright-field and high-resolution transmission electron microscopy studies of radiation damage induced by implantation of arsenic ions with 190 keV energy and 10^{14} cm⁻² fluence in MBE-grown HgCdTe film were performed. It was revealed that radiation damage penetrates substantially deeper than the projected ion range (250 and 93 nm, respectively). Unexpectedly, three separate defect layers were found in the damaged area. A 50 nm-thick sub-surface layer had very low defect density. The main defects in two layers that lied deeper were dislocation loops of different sizes: large dislocations loops with

low density, located at the depth 50–170 nm and small dislocations loops located at the depth 170–250 nm. The maximum density of dislocation loops was located at the depth 110 nm and was deeper than R_p , which confirmed the ballistic effect of the implantation process. In addition, different clusters of defects (vacancies, dopants, Ga atoms used in the preparation of TEM foils) and structural defects (stacking faults, nano-twins, dislocations) were observed in the radiation-damaged area.

After activation annealing, residual defects were still visible in the radiation-damaged area. Although, as before, it was still possible to distinguish three main layers, their thicknesses and the nature of defects were radically changed. The thickness of the sub-surface layer with low defect density decreased down to 10 nm, and that of the transition layer, on the contrary, increased up to 170 nm. The layer with large dislocation loops with low density underwent major changes: its thickness decreased down to 60 nm, and the dislocations loops transformed into dislocations with high density, $\sim 7.7 \times 10^9$ cm⁻². The maximum dislocation density was observed at the depth of 40 nm. Thus, the process of reconstruction of the crystalline structure under annealing proceeded in the direction from the depth to the surface via transport, transformation and annihilation of radiation-induced defects.

References

- Bommena R, Ketharanathan S, Wijewarnasuriya PS et al (2015) High-performance MWIR HgCdTe on Si substrate focal plane array development. *J Electron Mater* 44:3151–3156
- Gravrand O, Destefanis G (2013) Recent progress for HgCdTe quantum detection in France. *Infr Phys Technol* 59:163–171
- Izhnin II, Fitsych EI, Voitsekhovskii AV et al (2017a) Defects in arsenic-implanted p^+-n and n^+-p structures based on CdHgTe MBE films. *Russ Phys J* 60:92–97
- Izhnin II, Voitsekhovskii AV, Kororaev AG et al (2017b) Optical and electrical studies of arsenic-implanted HgCdTe films grown with molecular beam epitaxy on GaAs and Si substrates. *Infr Phys Technol* 81:52–58
- Kerlain A, Brunner A, Sam-Giao D et al (2016) Mid-wave HgCdTe FPA based on P on N technology: hot recent developments. NETD: dark current and 1/f noise considerations. *J Electron Mater* 45:4557–4562
- Lobre C, Jalabert D, Vickridge I et al (2013) Quantitative damage depth profiles in arsenic implanted HgCdTe. *Nuclear Instr Methods in Phys Res B* 313:76–80
- Lobre C, Jouneau P-H, Mollard L et al (2014) Characterization of the microstructure of HgCdTe with p -type doping. *J Electron Mater* 43:2908–2914
- Mollard L, Destefanis G, Bayer N et al (2009) Planar p -on- n HgCdTe FPAs by arsenic ion implantation. *J Electron Mater* 38:1805–1813
- Mollard L, Destefanis G, Bourgeois G et al (2011) Status of p -on- n arsenic-implanted HgCdTe technologies. *J Electron Mater* 40:1830–1839

- Umeda T, Toda A, Mochizuki Y (2004) Measurement of process-induced defects in Si sub-micron devices by combination of EDMR and TEM. *Eur Phys J Appl Phys* 27:13–19
- Yakushev MV, Brunev DV, Varavin VS et al (2011) HgCdTe heterostructures on Si(310) substrates for MWIR infrared photodetectors. *Semiconductors* 45:385–391

Publisher's note Springer Nature remains neutral with regard to jurisdictional claims in published maps and institutional affiliations.